

Compensation of electrical current drift in human–robot collision

Vinh Nguyen¹ · Jennifer Case²

Received: 21 July 2022 / Accepted: 24 October 2022 / Published online: 5 November 2022
© The Author(s), under exclusive licence to Springer-Verlag London Ltd., part of Springer Nature 2022

Abstract

Human–robot collaborative systems are being increasingly adopted in manufacturing environments due to their application flexibility, adaptability, and cost-effectiveness. The majority of robotic systems use electrical current sensors to measure joint torque in industrial robot arms and limit the robot's impact in the event of an unanticipated acceleration/deceleration, such as in the event of a collision with a human operator. However, these electrical current sensors are known to experience sensor drift, which results in measurement inaccuracy that can result in improper joint-torque or end-effector force readings. This paper provides a method to compensate for electrical current drift using a neural network-based controller to control robot velocity. To evaluate the compensation method, an experimental setup was developed where a robot joint collided with the biofidelic test device that mimics the deformation response of the human forearm while simultaneously measuring deformation and contact force using an embedded soft force sensor. The proposed method was shown to compensate for electrical current drift and therefore reduce resulting contact forces between the robot and the biofidelic test device. Hence, this research provides a method to quantify the behavior of electrical current sensor drift on human–robot collision and presents a data-driven methodology for compensation.

Keywords Degradation · Biofidelic sensors · Collaborative robots · Neural network · Electrical current

1 Introduction

Collaborative robots are being increasingly adopted by manufacturers due to their application flexibility, adaptability, and cost-effectiveness. Many of these robot designs use electrical current sensors housed in their joints as a method to infer torques experienced by each joint. The sensors can then be used for applications including end-effector force estimation [1], payload gravity compensation [2], and compliant teach-point programming [3]. In addition, one of the most critical applications of electrical current sensors is force-limiting control in the event of collisions with humans [4] where the safety stops triggered in risk assessments and general operation of the robot rely on the electrical current sensor measurements. Specifically, to

ensure safe human–robot interaction, existing safety standards, such as ISO/TS15066, have specified biomechanical force and pressure limits in the event of human–robot collision [5] and require that risk assessments be performed to identify worst-case human–robot collisions followed by validation testing to verify that resulting forces and pressures at the collision points do not exceed the biomechanical limits as specified per body region. Pre-evaluation of conditions that result in human–robot collision have been noted in prior literature based on the ISO/TS15066 [6]. For instance, researchers have developed a finite element model to calculate hazardous conditions in the event of human–robot contact [7]. In addition, researchers have also created experimental tests in human–robot collision where the robot collided with a leather ball and plastic cylinder for pre-evaluation purposes [8].

Repeated use of industrial robots results in performance degradation and susceptibility to sensor drift [9]. Most industrial robot performance research is focused on positional accuracy and repeatability involving the use of physical detection systems [10] and machine vision [11]. For instance, in one study, sensors were placed on humans and the robot was trained to use people's positions and

✉ Vinh Nguyen
vinhn@mtu.edu

¹ Department of Mechanical Engineering-Engineering Mechanics, Michigan Technological University, Houghton, MI 49931, USA

² Intelligent Systems Division, National Institute of Standards and Technology, Gaithersburg, MD 20899, USA

physiological reactions to change control strategies for collision avoidance [12]. In addition, a vision-guided collision avoidance system was proposed by monitoring both the human and the worker to send adjusted control commands in the event of a prediction collision [13]. However, the study of robot performance relative to electrical current sensor drift in industrial robots has not been examined as thoroughly despite typical datasheets indicating electrical current sensor drift as high as 5.7% [14], which could possibly be the result of temperature variations inherent to high-power applications. Though researchers have demonstrated a variety of techniques to study human–robot collision including proposing operating procedures [15], alternate control strategies [16], and using joint velocity and current measurements to minimize impact [17], studies of the effects of electrical current drift on human–robot collision control are limited. Because electrical current sensors measurements provide the fundamental data from which force-limiting control is implemented, errors in the electrical current sensor measurements due to drift can adversely influence applications such as the impact in the event of human–robot collision.

The paper aims to compensate for electrical current degradation in collaborative robots using a neural network-based controller for applications including force limiting control during human–robot collisions. To conduct this study, an experimental setup was developed to mimic a case study where the joint of a collaborative robot collides with a surrogate human forearm. A biofidelic test device incorporating a soft capacitive sensor with similar material properties to that of the human forearm is used to measure the force and deformation that would be experienced by an operator [18]. Multiple collision experiments were conducted at various joint velocities measured by the UR10 to train a neural network to predict the approximate velocity based on current, joint position, and time measurements. The predicted velocity was then used to infer error in velocity, which was used by a proportional-integral-derivative (PID) controller to reduce the influence of electrical drift. It was shown that electrical current drift of the sensors resulted in significant changes in force during impacts with the biofidelic test device and the neural network-based compensation method reduced the effect of electrical current drift, thereby reducing contact forces.

2 Compensation methodology

To reduce the influence of electrical current drift, this paper uses a neural network trained by robot collisions with the biofidelic device to infer the joint velocity errors for use in a PID controller to control joint velocity. Note that the implementation of the controller can also be used in applications that are

subject to errors in electrical current measurements outside of human–robot collision, such as force control and gravity compensation.

Researchers primarily use electrical current to predict outputs including joint torque and end-effector forces. This work attempts to predict the joint velocity errors based on electrical current data, from which prior research is limited. Thus, we use a neural network [19] to predict the assumed joint velocity based on time, joint position, and electrical current data as inputs. Though other data-driven methods exist, neural networks have been demonstrated to outperform naïve Bayes [20] and random forest [21] in prior literature. Furthermore, a neural network was demonstrated to exhibit the fastest prediction time compared to the aforementioned data-driven models [22] and therefore is able to satisfying the timing requirements for real-time control. In addition, neural networks have been previously demonstrated in human–robot collision detection applications [23]. The neural network in this work consists of one hidden layer with 10 nodes and rectified linear unit activation functions. The aforementioned parameters were used as inputs into the MATLAB function `fitrnet()`. While electrical current can be used as the output of the neural network and input into a PID controller, current sensor readings based on velocity, position, and time are not unique, and therefore errors in current readings can result nonlinear behavior that can influence stability and accuracy of a PID controller [24]. In addition, electrical current is not a stable output and can therefore affect the stability of the PID controller.

To compensate for current drift, the neural network was implemented in the controller shown in Fig. 1. The controller operates by moving the robot at an initial fixed joint velocity. As the joint position changes, electrical current (filtered by a 40-point window median filter [25]) and time data are collected and used as inputs to the neural network. The median filter for electric current is intended to filter a sudden increase in current in the event of a collision to reduce possible harm to the human operator. If the electrical current is incorrect (for instance, due to drift), then the neural network will predict the corresponding velocity. The difference between the instantaneous velocity and the predicted velocity is then inputted into a PID algorithm with the result being added onto the instantaneous velocity. This new command velocity is then inputted into the robot controller to adjust the speed of the robot. By directly controlling the joint velocity, this approach compensates for error in electrical current drift.

3 Experimental setup

This section describes the design of biofidelic device and the experimental setup for performing robot collisions as shown in Fig. 2.

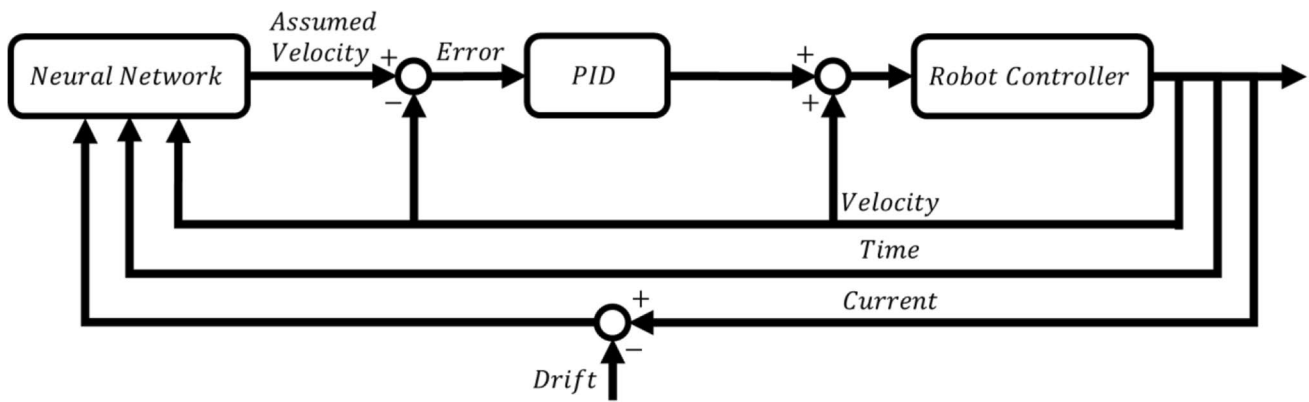


Fig. 1 Diagram of proposed controller used in this work

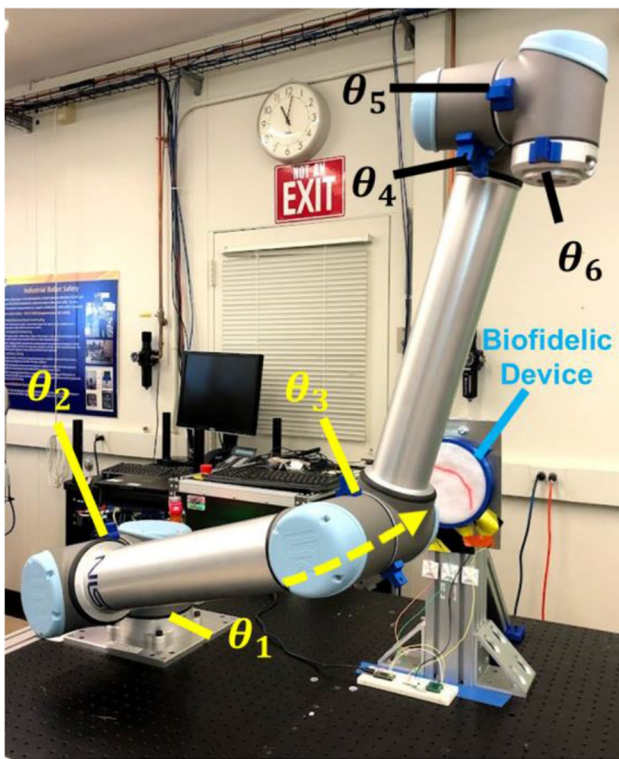


Fig. 2 Experimental setup for testing collisions between the robot and biofidelic device

3.1 Robotic system

In this work, a collaborative robot (UR10 CB3-series, Universal Robots) was used to collide with a biofidelic device. Robot communication was conducted using user datagram protocol (UDP) with data being read by the computer and commands being sent to the robot using the real-time data exchange (RTDE) and the URScript formats, respectively, with a cycle time of 10 ms.

The joint angles $[\theta_2 \dots \theta_6]$ were fixed to be $[-162.73^\circ, 55.77^\circ, -166.63^\circ, -90.00^\circ, 0.00^\circ]$, while the robot was driven to rotate about θ_1 at a fixed velocity in the direction shown in Fig. 2. As the robot rotates about θ_1 , it will collide with the biofidelic device. At this point, the current sensor measurements will sharply increase as shown in Fig. 3. Note that the robot automatically halts movement if the electrical current increases above a factory-set threshold or if the robot's position significantly deviates from its intended path. However, to minimize safety hazards and avoid permanent damage to the robot, the robot was configured to halt movement if the current in Joint 1 exceeded 1.75 Amps. Thus, if the current drifts such that measurements are inaccurately lower than the correct values, the robot would take longer to exceed 1.75 Amps, resulting in more force and deformation experienced by the biofidelic device. Because studies of the current degradation of industrial robots are limited, the current drift is simulated as a set rate during the operation. In addition, the simulated drift is assumed to be the sole source of electrical current degradation.

3.2 Biofidelic device

To demonstrate an application for the proposed electrical current compensation method used to reduce errors in electrical current and therefore human–robot collision force, a biofidelic device was used to mimic the human forearm. To fabricate the biofidelic device, a soft capacitive sensor was manufactured using conductive fabric as electrodes and elastomer as a dielectric. Figure 4 shows the fabrication process for these sensors; it should be noted that the fabrication procedure of the soft capacitive sensor in this work follows prior work by the authors [18]. The sensor fabrication involves a two-step molding process utilizing acrylic molds and conductive fabric (Nora Dell, Shieldex)

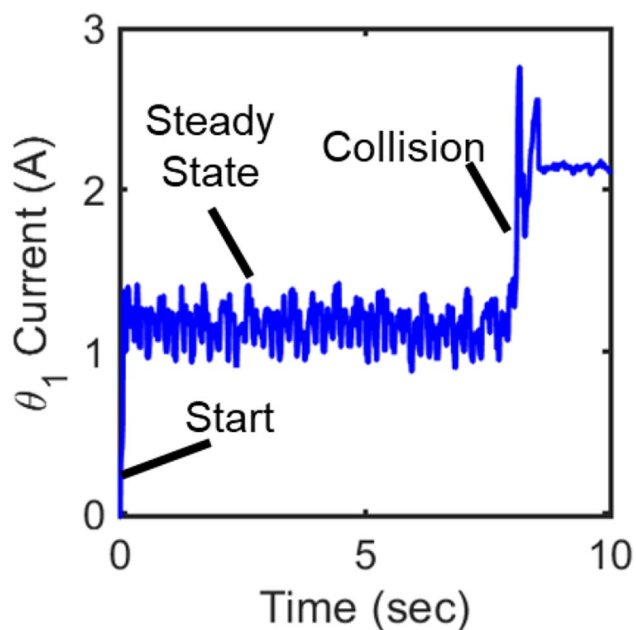


Fig. 3 Example raw current reading during robot-biofidelic device collision

that were cut using a laser cutter (universal laser system) alongside the dielectric elastomer (EcoFlex 00–10, Smooth-On, Inc.). The initial mold has the conductive fabric electrodes patterned between the pieces of acrylic with all parts being held in place with sewing pins. With the conductive fabric electrodes separated, the dielectric elastomer was poured into the mold and then cured for at least 24 h. After

curing, the mold was disassembled, the excess elastomer was removed from the sensor, and the conductive fabric was trimmed to create alternating tabs. A second mold was created to fully encapsulate the conductive fabric to prevent delamination. The sensor was placed in the mold and held in place with a 3D-printed part. Additional EcoFlex 00–10 elastomer was poured around the sensor and allowed to cure for at least 24 h. After disassembling the second mold and removing excess elastomer, conductive thread (Stainless Thin Conductive Thread, Adafruit, Inc.) was sewn through either side of the sensor to connect the alternating layers of conductive fabric completing the capacitive sensor. For this paper, the sensor consisted of seven electrodes and, therefore, six dielectric layers. The active area of the sensor is 1 cm × 1 cm with the overall sensor dimensions of 1.8 cm × 1 cm × 1.2 cm.

To complete the biofidelic device (shown in Fig. 5), the sensor was embedded into bulk elastomer (P-10, Silicones, Inc.) with a foam sheet (Soma Foama 15, Smooth-On, Inc.) acting as a soft skin on top of the elastomer and sensor. This design replicates force–displacement characteristics of the human forearm. The bulk elastomer has a diameter of 14.25 cm with a hole in the center for the sensor and is 1.12-cm thick, and the foam sheet is also 1.12-cm thick.

Because of the design of the sensors, each of the electrodes can be treated as parallel plates spaced by dielectrics with initial thicknesses; thus, the sensor can be treated as a stacked parallel plate capacitor [26]. In the case of human–robot collision, the capacitance will change as the sensor is compressed and the thickness of the dielectric

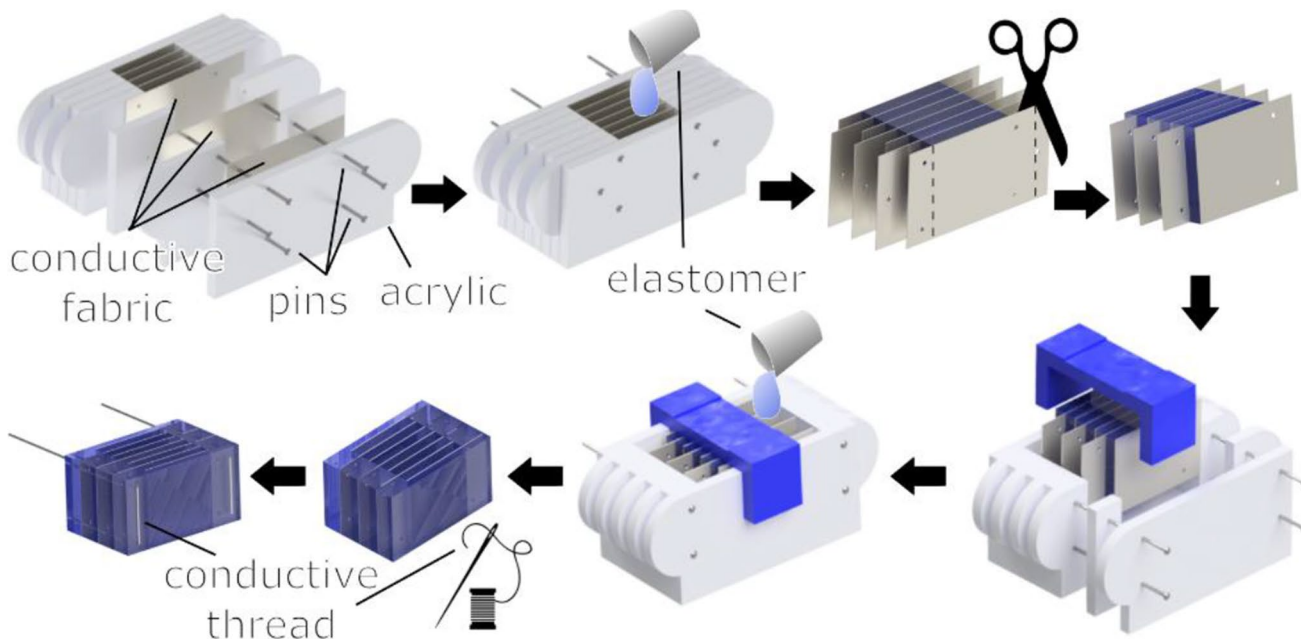
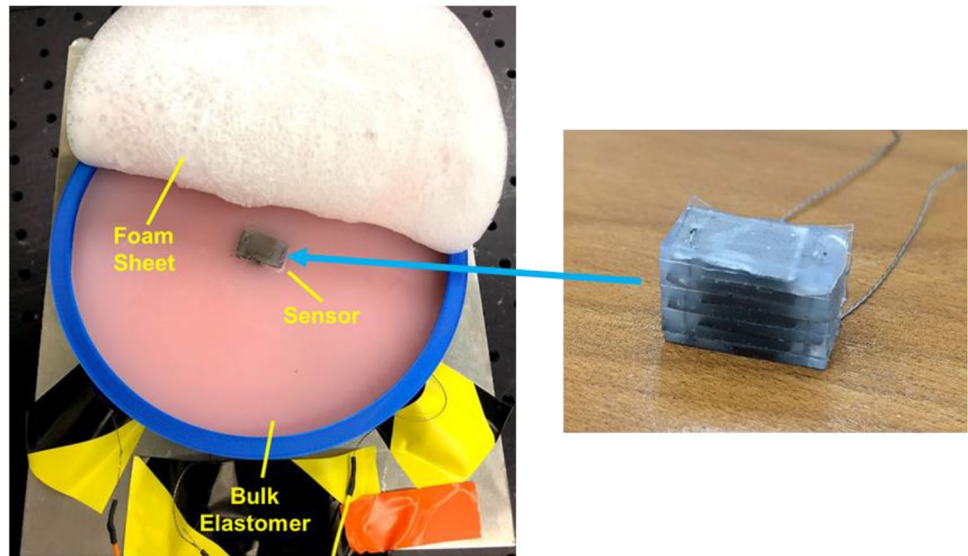


Fig. 4 Mold based fabrication process of soft capacitive sensor

Fig. 5 Opened setup of biofidelic device

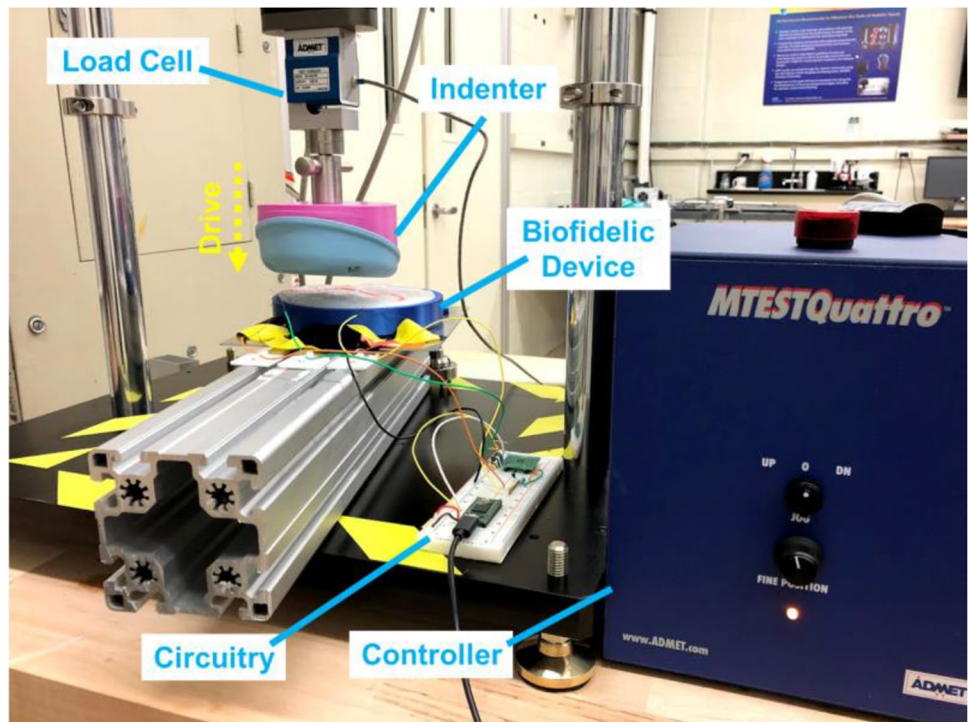


decreases. In this work, the capacitance is assumed to change linearly with the applied force and deformation. A circuit was built to measure the capacitance where a capacitance-to-digital converter (FDC2214, Texas Instruments) was used to measure the capacitance of the sensor at a rate of 250 Hz. In addition, a 1 nF capacitor was wired in series with the sensor to protect the circuit against electrical shorts between the conductive fabric.

To correlate the force and deformation to measured capacitance, the biofidelic device was mounted in a material

testing machine (eXpert 5600, Admet Solutions) as shown in Fig. 6. The indenter of the materials testing machine was adapted to mimic a joint collision by mounting the elbow cap of the UR10 onto a 3D-printed mount. The indenter was driven into the biofidelic device at a speed of 100 mm/min until numerous predetermined force thresholds were measured by the materials testing machine. The nominal forces for these experiments were 20 N, 30 N, 40 N, 50 N, and 60 N. At each stop, the deformation, steady-state force, and the raw 28-bit integer value output by the FDC2214

Fig. 6 Calibration setup of biofidelic device



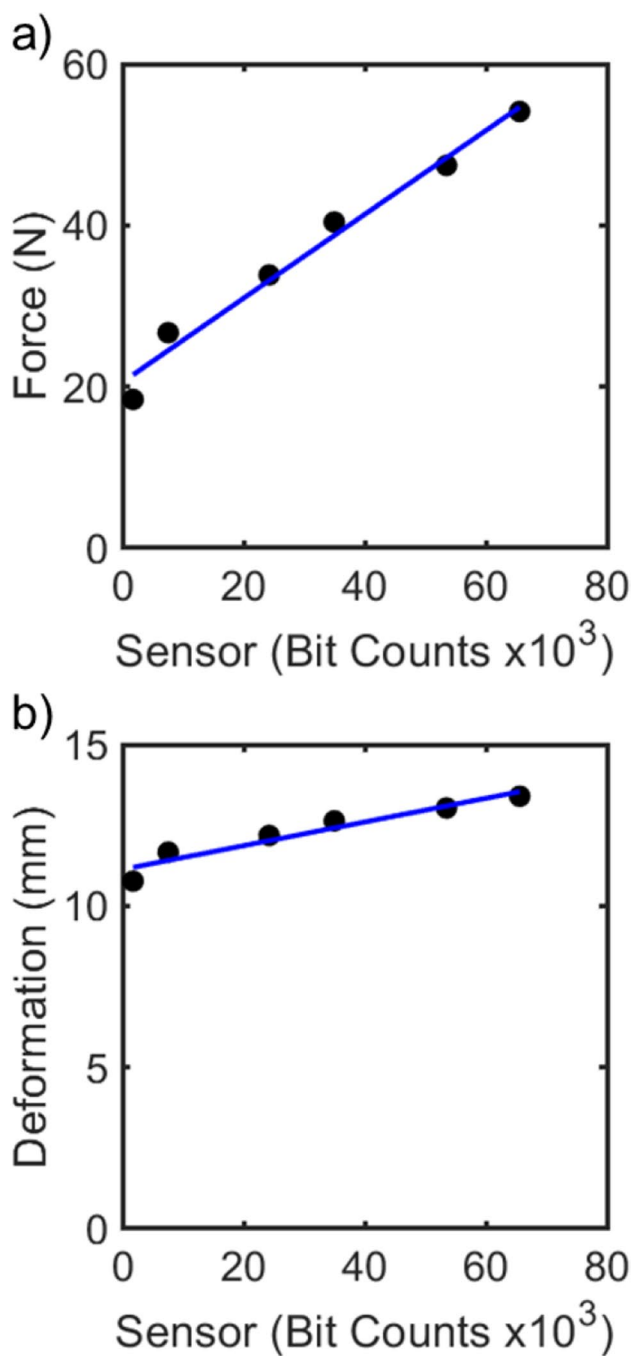


Fig. 7 Calibration curves of the biofidelic sensor for **a** force and **b** displacement and corresponding linear fits

were measured by a Data Acquisition System (USB-6363, National Instruments) at 1000 Hz for 2 s. Note that the difference between the sensor readings at the beginning of the test and the steady-state compressed state was used for calibration and computation to remove the influences of plastic deformation and viscoelastic behavior of the biofidelic device and the weight of the foam sheet on the sensor.

Figure 7 shows the force and deformation calibration curves for the biofidelic sensor. Note that as the applied force increases, the spacing between the electrodes in the sensor decreases. This decrease in spacing corresponds to an increase in change in capacitance which results in an increase in the raw bit count values. The error in the force and deformation linear fits are shown to be correlated with coefficient of determination (R^2) values of 0.98 and 0.92, respectively, demonstrating that the assumption of linearity holds for both force and deformation. The linear fits for the force and deformation behaviors of the sensor are $0.00052sensor + 20.56$ and $3.67 * 10^{-5}sensor + 11.13$, respectively. It should be noted that nonlinear behavior is expected to occur in the lower force range of approximately < 10 N due to the deformation of the foam. However, the forces measured in this paper are expected to be well above that range, and therefore linear behavior was observed at the maximum impact force ranges.

4 Results

To train the neural network, tests were conducted by driving the robot to collide with the biofidelic device and stop motion after 1.75 Amps. Using the biofidelic device, joint speeds at $1^\circ/sec$, $3^\circ/sec$, $5^\circ/sec$, and $7^\circ/sec$, with three replications each, were tested with no simulated drift to record data for neural network calibration. Replications were conducted to account for possible noise errors in the electrical current measurements. In this work, fivefold cross-validation was conducted to evaluate the model, thus resulting in an

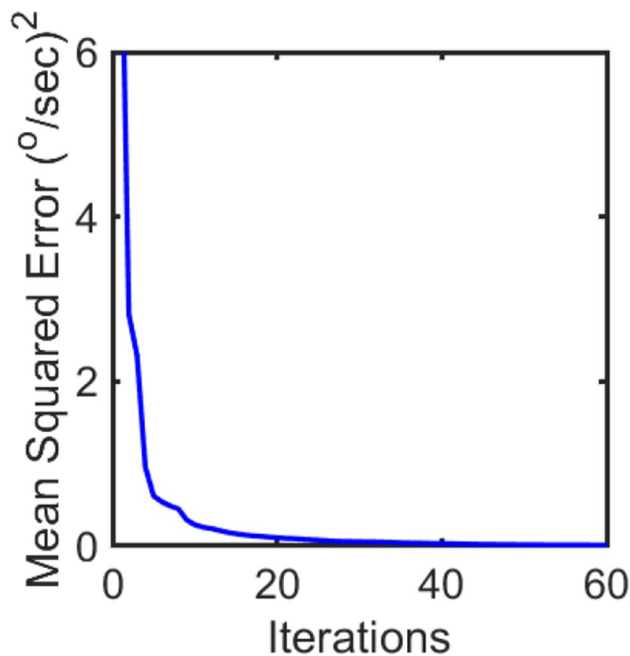


Fig. 8 Mean squared error plot from cross validation

80% to 20% training-to-testing points partition. The plot of mean squared error from the cross validation is plotted in Fig. 8, and the mean squared error is shown to converge to 0.0027 ($^{\circ}/\text{sec}$)² as iterations increase, demonstrating appropriate selection of the activation function and layer parameters. Also, the R^2 was calculated to be 0.97, which means that the error is uncorrelated, and the model captures the majority of known trends in the data. Hence, the neural network and the training data used in this work were sufficient for accurate joint velocity calculations.

To examine the performance of the compensation methodology, the robot was used to conduct the same experimental procedure as the neural network calibration with a speed of $4^{\circ}/\text{sec}$. Varying degrees of simulated drift rate (0 mA/sec, 30 mA/sec, 60 mA/sec, and 90 mA/sec) were tested. Note that the tested amount of simulated drift in this work is expected to be significantly more than expected in normal operation in a production facility and that this severity of the drift is chosen to efficiently evaluate the influence of current drift and the performance of the compensation method.

Figure 9 shows representative time series data for filtered current (top row) and sensor measurements (bottom row). When there is no drift (0 mA/sec), then the compensation method appears to result in similar time series for the filtered current measurements in addition to the sensor readings settling at similar points after collision. When the drift rate increases to 30 mA/sec, then the compensation method reduces the drift in the current sensor mildly, which is reflected in a minor decrease in the sensor reading. In addition, without compensation, the sensor reading at a

drift rate of 30 mA/sec appears to settle at a larger value than at 0 mA/sec. As the drift rate increases dramatically to 90 mA/sec, the compensation method can reduce the drift more significantly with a more dramatic reduction in sensor readings. Note that for all cases when drift is introduced, the compensation method does not completely remove current drift. This can be mitigated by tuning the PID gains (specifically, the P gain) at the cost of more sensitivity to noise when there is no drift. In addition, note that production environments are expected to experience less electrical current drift and the compensation effort is expected to be much less than the 60 mA/sec and 90 mA/sec cases.

Figure 10 shows the final steady-state (a) force and (b) deformation experienced by the biofidelic device. As expected, when not using compensation, the collision force increases as the current drift increases. In addition, the deformation of the biofidelic device without compensation is also shown to increase, though only from 8.47 mm to 10.03 mm. While this seems like a small change in deformation, as flesh deforms, at some point, small changes in deformation result in significant changes in force. However, when using compensation, the collision force is shown to be constant with respect to the drift rate, thus demonstrating the compensation method's capability to reduce the collision force in the event of an impact. In addition, the compensation method is demonstrated to ensure that the deformation remains similar for differing severities of electrical current drift. Also, the standard deviations of the trials appear to be more consistent when using the compensation as opposed to without using compensation. Thus, the results show that electrical current drift can increase the collision force and deformation experienced in

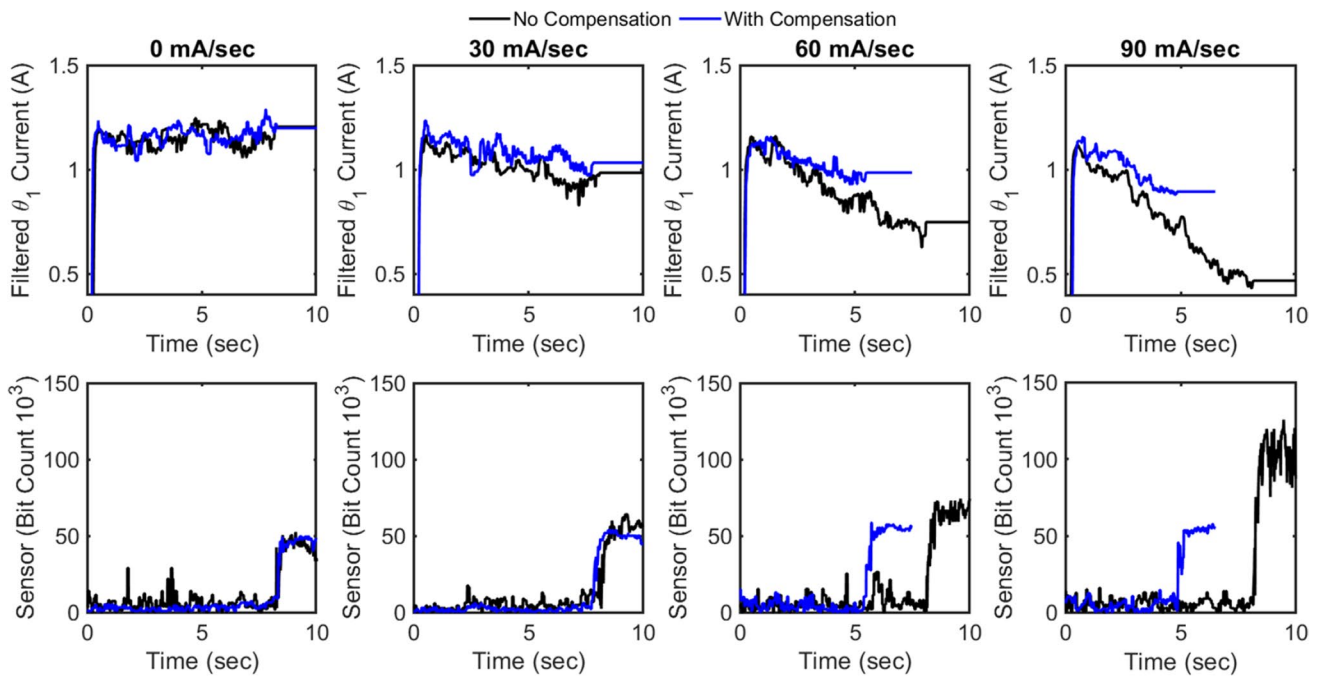


Fig. 9 Representative time series data for filtered current (top row) and sensor measurements (bottom row)

human–robot collision and therefore should be considered when designing collaborative robots. In addition, the results also show that the compensation process used in this work is a plausible methodology to compensate for electrical current drift.

For this specific experimental setup, the required electrical current levels to exceed the biomechanical limits specified by ISO/TS15066 were calculated. Referring to ISO/TS15066, the maximum force limit for a human forearm is 160 N. A linear fit between the experienced force (Fig. 10) and steady-state electrical current (Fig. 9) without compensation was determined to be $-0.0296 * force + 2.604$ with an R^2 of 0.95. Hence, the steady-state electrical current in θ_1 required to breach the biomechanical limit was calculated to be -2.13 Amps. Thus, the corresponding cumulative electrical current drift starting from a 0 mA/sec drift value of 1.21 Amps (Fig. 9) was determined to be 3.34 Amps. Note that the electrical current sensor drifting 3.34 Amps, and thus breach the biomechanical limit, would be considered unrealistic. However, the drift threshold would also depend on the experimental setup. Hence, this paper also provides a method to determine the acceptable electrical current drift for a given application based on biomechanical limits.

5 Conclusion

This paper provides the use of a biofidelic device with an embedded capacitive sensor to train a neural network implemented in a PID controller to compensate for the influence of electrical current drift. The results showed that the proposed controller method led to reduced collision force and deformation by compensating for simulated electrical current drift. Furthermore, by demonstrating that the compensation method resulted in noticeable impacts on the biofidelic device, the results showed that electrical current drift experienced by industrial robots can significantly influence collision forces and deformation. Hence, this research demonstrates a compensation method for human–robot collision in the event of electrical current drift in addition to presenting an offline system for training and evaluating methods in human–robot collision. Specifically, this research also addressed the limitations of offline experimental setups for evaluating human–robot collision by utilizing a biofidelic sensor to measure force and deformation.

Note that the human response will vary significantly depending on human size and location of impact. Thus, a limitation of this work is the analysis on a single human setup. Furthermore, multiple points of the robot can collide with a human, and therefore more analysis must be conducted for the future robot points of contact as well. In addition, redundant electrical current sensors are highly recommended for future work to detect and compensate for drift at the measurement stage. The internal electrical current sensors in industrial robots are designed to

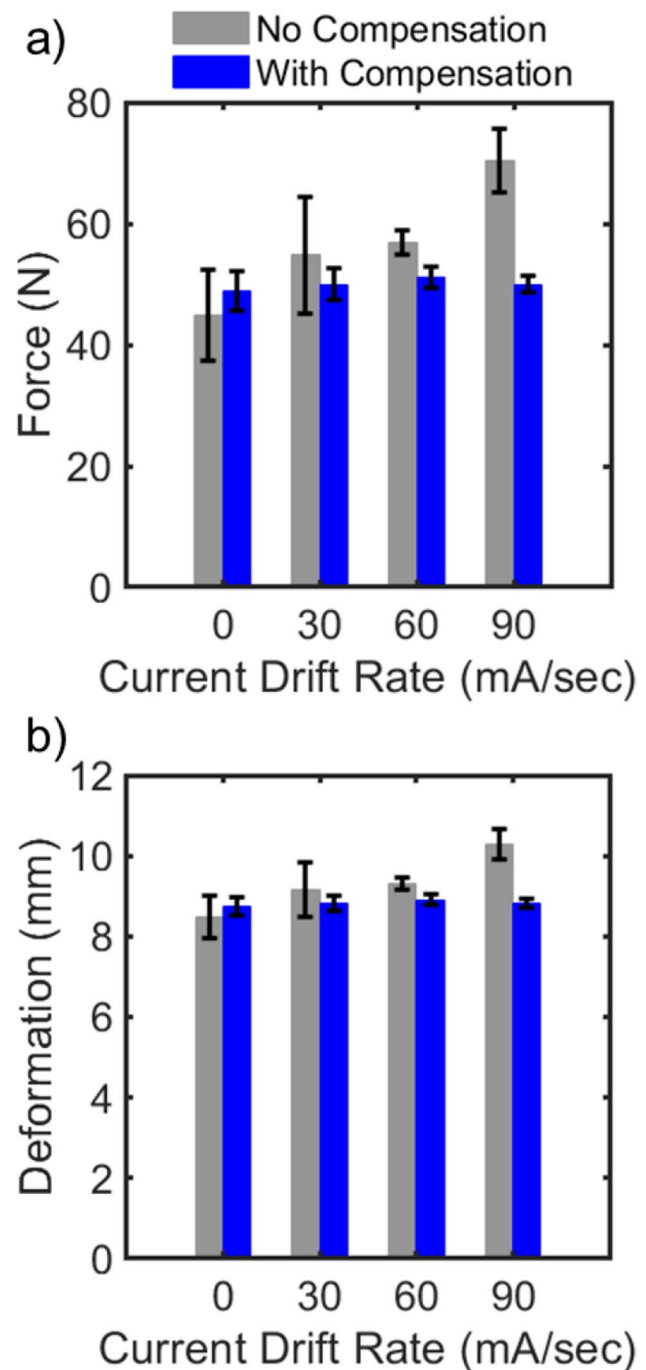


Fig. 10 Resulting **a** force and **b** deformation experienced by the biofidelic device. Error bars are ± 1 standard deviation

be cost-effective, and therefore more electrical current sensors are critical for verifying the accuracy of the internal electrical current sensors themselves. Note that electrical current drift is a general condition that can occur in fields of robotics not exclusive to human–robot collision. Thus, the compensation method in this work can apply to general inaccuracies in electrical current sensors in industrial robots for further studies, including force and gravity compensation or teach-point programming.

Author contribution All authors contributed to the study conception and design. Material preparation and calibration were performed by Jennifer Case. Experimental setup and data collection were performed by Vinh Nguyen. The first draft of the manuscript was written by Vinh Nguyen, and all authors commented on previous versions of the manuscript. All authors approved the final manuscript.

Funding This work was funded by the National Institute of Standards and Technology and the National Research Council Research Associateship Program.

Declarations

Competing interests The authors declare no competing interests.

Disclaimer Certain commercial entities, equipment, or materials may be identified in this document in order to describe an experimental procedure or concept adequately. Such identification is not intended to imply recommendation or endorsement by the National Institute of Standards and Technology, nor is it intended to imply that the entities, materials, or equipment are necessarily the best available for the purpose.

References

1. Wahrburg A, Bös J, Listmann KD, Dai F, Matthias B, Ding H (2017) Motor-current-based estimation of cartesian contact forces and torques for robotic manipulators and its application to force control. *IEEE Trans Autom Sci Eng* 15(2):879–886. <https://doi.org/10.1109/TASE.2017.2691136>
2. Arakelian V (2016) Gravity compensation in robotics. *Adv Robot* 30(2):79–96. <https://doi.org/10.1080/01691864.2015.1090334>
3. de Gea FJ et al (2017) Multimodal sensor-based whole-body control for human–robot collaboration in industrial settings. *Robot Auton Syst* 94:102–119. <https://doi.org/10.1016/j.robot.2017.04.007>
4. Aivaliotis P, Aivaliotis S, Gkournelos C, Kokkalis K, Michalos G, Makris S (2019) Power and force limiting on industrial robots for human–robot collaboration. *Robot Comput-Integr Manuf* 59:346–360. <https://doi.org/10.1016/j.rcim.2019.05.001>
5. ISO/TS 15066:2016 Robots and robotic devices — collaborative robots (2016) <https://www.iso.org/standard/62996.html>. Accessed 1 June 2022
6. Chemweno P, Pintelon L, Decre W (2020) Orienting safety assurance with outcomes of hazard analysis and risk assessment: a review of the ISO 15066 standard for collaborative robot systems. *Saf Sci* 129:104832. <https://doi.org/10.1016/j.ssci.2020.104832>
7. Shin H, Kim S, Seo K, Rhim S (2019) A real-time human–robot collision safety evaluation method for collaborative robot. *Third IEEE Int Conf Robot Comput (IRC) 2019*:509–513. <https://doi.org/10.1109/IRC.2019.00106>
8. Cordero CA, Carbone G, Ceccarelli M, Echávarri J, Muñoz JL (2014) Experimental tests in human–robot collision evaluation and characterization of a new safety index for robot operation. *Mech Mach Theory* 80:184–199. <https://doi.org/10.1016/j.mechmachtheory.2014.06.004>
9. Qiao G, Weiss BA (2017) Accuracy degradation analysis for industrial robot systems. *Int Manuf Sci Eng Conf: V003T04A006*. <https://doi.org/10.1115/MSEC2017-2782>
10. Algburi RNA, Gao H (2019) Health assessment and fault detection system for an industrial robot using the rotary encoder signal. *Energies* 12(14):2816. <https://doi.org/10.3390/en12142816>
11. Izagirre U, Andonegui I, Eciolaza L, Zurutuza U (2021) Towards manufacturing robotics accuracy degradation assessment: a vision-based data-driven implementation. *Robot and Comput-Integr Manuf* 67:102029. <https://doi.org/10.1016/j.rcim.2020.102029>
12. Kulić D, Croft E (2007) Pre-collision safety strategies for human–robot interaction. *Auton Robot* 22(2):149–164. <https://doi.org/10.1007/s10514-006-9009-4>
13. Wang L, Schmidt B, Nee AY (2013) Vision-guided active collision avoidance for human–robot collaborations. *Manuf Lett* 1(1):5–8. <https://doi.org/10.1016/j.mfglet.2013.08.001>
14. Allegro Microsystems (2021) ACS71240 Datasheet. <https://www.allegromicro.com/-/media/files/datasheets/acs71240-datasheet.pdf>. Accessed 1 June 2022
15. Indri M, Trapani S, Lazzerio I (2015) A general procedure for collision detection between an industrial robot and the environment. *IEEE 20th Conf Emerg Technol Fact Autom (ETFA)*: 1–8. <https://doi.org/10.1109/ETFA.2015.7301539>
16. Haddadin S, Albu-Schaffer A, De Luca A, Hirzinger G (2008) Collision detection and reaction: a contribution to safe physical human–robot interaction. *IEEE/RSJ Int Conf Intell Robot Syst*: 3356–3363. <https://doi.org/10.1109/IROS.2008.4650764>
17. Geravand M, Flacco F, De Luca A (2013) Human–robot physical interaction and collaboration using an industrial robot with a closed control architecture. *IEEE Int Conf Robot Autom*: 4000–4007. <https://doi.org/10.1109/ICRA.2013.6631141>
18. Case JC, Rangarajan N, Falco J, and Kimble K (2022) Towards the development of soft force and pressure sensors for robot safety applications. *IEEE Sensors*: 1–4. <https://doi.org/10.1109/SENSORS47087.2021.9639838>
19. Anthony M, Bartlett PL, Bartlett PL (1992) *Neural network learning: theoretical foundations*. Cambridge, New York
20. Saritas MM, Yasar A (2019) Performance analysis of ANN and Naive Bayes classification algorithm for data classification. *Int J Intell Syst Appl Eng* 7(2):88–91. <https://doi.org/10.18201/ijisae.2019252786>
21. Kayri M, Kayri I, Gencoglu MT (2017) The performance comparison of multiple linear regression, random forest and artificial neural network by using photovoltaic and atmospheric data. *14th Int Conf Eng Mod Electr Syst (EMES)*: 1–4. <https://doi.org/10.1109/EMES.2017.7980368>
22. Nguyen V, Marvel J (2022) Evaluation of data-driven models in human–robot load-sharing. *Int Manuf Sci Eng Conf* 85819:V002T06A003 10.1115/MSEC2022-83907
23. Sharkawy AN, Aspragathos N (2018) Human–robot collision detection based on neural networks. *Int J Mech Eng Robot Res* 7(2):150–157. <https://doi.org/10.18178/ijmerr.7.2.150-157>
24. Zhou G, Birdwell JD (1992) PID autotuner design using machine learning. *IEEE Symp Comput-Aided Control Syst Des*: 173–179. <https://doi.org/10.1109/CACSD.1992.274411>
25. Arce G, McLoughlin M (1987) Theoretical analysis of the max/median filter. *IEEE Trans Acoust Speech Signal Proc* 35(1):60–69. <https://doi.org/10.1109/TASSP.1987.1165036>
26. Grove T, Masters M, Miers R (2005) Determining dielectric constants using a parallel plate capacitor. *Am J Phys* 73(1):52–56. <https://doi.org/10.1119/1.1794757>

Publisher's note Springer Nature remains neutral with regard to jurisdictional claims in published maps and institutional affiliations.

Springer Nature or its licensor (e.g. a society or other partner) holds exclusive rights to this article under a publishing agreement with the author(s) or other rightsholder(s); author self-archiving of the accepted manuscript version of this article is solely governed by the terms of such publishing agreement and applicable law.